



HAL
open science

Simultaneous temperature and thickness measurements of falling liquid films by laser-induced fluorescence

R. Collignon, Ophélie Caballina, F. Lemoine, Guillaume Castanet

► **To cite this version:**

R. Collignon, Ophélie Caballina, F. Lemoine, Guillaume Castanet. Simultaneous temperature and thickness measurements of falling liquid films by laser-induced fluorescence. *Experiments in Fluids*, 2022, 63 (4), pp.68. 10.1007/s00348-022-03420-x . hal-03648578

HAL Id: hal-03648578

<https://hal.science/hal-03648578>

Submitted on 21 Apr 2022

HAL is a multi-disciplinary open access archive for the deposit and dissemination of scientific research documents, whether they are published or not. The documents may come from teaching and research institutions in France or abroad, or from public or private research centers.

L'archive ouverte pluridisciplinaire **HAL**, est destinée au dépôt et à la diffusion de documents scientifiques de niveau recherche, publiés ou non, émanant des établissements d'enseignement et de recherche français ou étrangers, des laboratoires publics ou privés.

Simultaneous temperature and thickness measurements of falling liquid films by laser-induced fluorescence

R. Collignon¹, O. Caballina², F. Lemoine² and G. Castanet^{2*}

¹*Université Savoie Mont Blanc, CNRS, LOCIE, 73000 Chambéry, France*

²*Université de Lorraine, CNRS, LEMTA, 54000 Nancy, France*

**Corresponding author*

Abstract

Thin wavy liquid films are used in many applications as heat and mass transfer promoters thanks to their great performances for a small liquid consumption. To evaluate the influence of the coupling between the wavy fluid dynamics and the heat transfer in a 2D waves regime, a pointwise laser-induced fluorescence technique has been developed. The technique enables a simultaneous measurement of both the thickness and the temperature of a wavy film flowing down an inclined plane with a high temporal resolution thanks to an optical probe placed directly above the liquid film. The fluorescence intensity is integrated over the thickness of the film, allowing a robust measurement of temperature and thickness for strongly perturbed wave fronts. This paper reports on the development of the technique and discuss the capabilities and limits of the current design. Water liquid films were investigated under two-dimensional waves conditions. The measurements, and the evaluation of the local heat transfer coefficient they permit, reveal the regions where mixing is enhanced by convective circulation zones.

1 Introduction

Falling liquid films are found in a variety of processes involving heat and mass transfers such as evaporators or tubular exchangers. Wave formation on the surface of these films, which are inherently unstable, can significantly enhance heat and mass transfers compared to a smooth liquid film. (Yoshimura et al., 1996). To clarify the mechanisms leading to this enhancement, both theoretical (Miyara, 1999; Chhay et al., 2017; Chernyavskiy and Pavlenko, 2017; Cellier and Ruyer-Quil, 2020) and experimental (Schagen et al., 2006; Akesjo et al., 2015; Markides et al., 2016) studies have been conducted. However, despite ongoing efforts, further experimental developments are still needed to gain understanding on the wave-induced mixing inside the film and its effects on heat and mass transfers. Due to the inherent complexity of thin falling liquid films, spatially and temporally resolved measurements of the liquid temperature, remain a real challenge. Optical techniques are preferred as they are non-invasive, but the deformation of the film in the presence of surface waves can create strong optical distortions limiting the quantification capabilities of these techniques.

IR thermography, classically used to determine the temperature of solid surfaces (Al-Sibai et al., 2002; Mathie and Markides, 2013), has been adapted in several studies to evaluate the temperature of films (Chinnov and Shatskii, 2010; Chinnov et al., 2012; Chinnov and Abdurakipov, 2013; Chinnov, 2014; Chinnov and Abdurakipov, 2017; Lel et al., 2007, 2008). Spatially and temporally resolved measurements obtained by this method, proved the predominant role of thermocapillary forces driven by the wave-amplified surface temperature gradients. However, only the temperature at the surface or very close to it is accessible with this method. This means that assumption are needed to describe the temperature inside the of the liquid, which is a limitation for the understanding of the transfer phenomena that occur inside the film. As an alternative, the liquid temperature can be measured based on the luminescence (phosphorescence, fluorescence) of given species. Laser-induced fluorescence is a

versatile technique that was used to measure the temperature in different flow configurations including natural convective flows (Sakakibara and Adrian, 2004), turbulent liquid jets (Chaze et al., 2016), droplets and sprays systems (Dunand et al., 2012; Chaze et al., 2017; Stiti et al., 2021). In falling liquid films, a few examples of implementation can be pointed out. Schagen et al. (2006); Schagen and Modigell (2007) used both the phosphorescence and the fluorescence of biacetyl to measure the temperature profile and the thickness of the film with an intensity based method. They were able to show significant temperature differences inside the thickness of the liquid film, in particular a lower temperature in the hump of the wave. The fluorescence light intensity was used to infer the local film thickness, while the temperature was measured based on the intensity decay of the phosphorescence signal when travelling between two points separated by several millimeters. Due to the long-life phosphorescence of biacetyl, excited molecules of biacetyl move out of the observation volume due to the local flow velocity. This effect can be corrected provided the velocity profile inside the waves, which was not measured but inferred from assumptions in these studies. An oxygen-free aqueous solution is required to ensure a sufficient phosphorescence signal that only depends on temperature, as phosphorescence is typically influenced by the oxygen fraction in solution. Fluorescence does not suffer the same limitations than phosphorescence due to a much shorter lifetime (typically in the range of a few ns). Xue and Zhang (2018) employed laser-induced fluorescence (LIF) to investigate the heating in liquid films flowing down a transparent vertical tube. They were able to evidence spatial temperature gradients in the thickness of the film. The imaging technique they employed, is a one-color LIF method, as the fluorescence signal is integrated over the complete emission spectrum of rhodamine B. To be reliable, these measurements require perfectly controlled conditions and the utmost care to ensure that any variation in the LIF signal can be attributed to a change in temperature. Thus, measurements by Xue and Zhang (2018) were restricted to perfectly flat film. Mathie et al. (2013); Markides et al. (2016) and Charogiannis et al. (2016) also used rhodamine B and one-color approach to determine the liquid temperature in a thin layer close to the film surface. Thanks to a very high concentration of rhodamine B (around 1 g/L) and thus to a very high absorption of the wavelength of the laser, they were able to restrict the measurement volume to a thin layer of liquid under the free surface, where the laser light is strongly absorbed by the dye solution.

In an effort to resolve temperature gradients inside the film, Collignon et al. (2021) recently developed a planar imaging technique based on the intensity ratio of two spectral detection bands (two-color PLIF technique). The falling liquid film was illuminated by a pulsed laser sheet perpendicular to the wall while two cameras were used to capture simultaneous images of the fluorescence intensity signal in the two detection bands. The temperature fields could be derived with a great accuracy, since most of the optical disturbances induced by the waves were eliminated in the pixel-to-pixel ratio. Highly magnified images (with a field of view substantially smaller than the wavelength of the perturbations) were recorded at different times. Then, the instantaneous temperature field in the whole wave was reconstructed knowing the time delay between the images. This approach was successful in evidencing mixing zones and temperature gradients in the case of periodical waves, since the reconstruction requires a perfect regularity of the waves to combine the images together. This method, however, is difficult to implement in strongly perturbed cases and quickly showed limitations for the study of unsteady wave fronts. A new approach was thus needed to explore a broader space of perturbation cases. The technique developed in the present study is also an implementation of laser-induced fluorescence to measure the temperature within the thickness of liquid films. The two-color LIF technique is implemented as a pointwise technique by focusing the laser beam in a precise region of the flow. Thus, it is not intended to characterize thermal gradients along the film thickness like in Collignon et al. (2021), but to monitor the time evolution of the thickness-averaged temperature at a given position in the film flow. Many approaches can be used to determine the local thickness of liquid films, including CCI (Confocal Chromatic Imaging) technique (Cohen-Sabban et al., 2001; Lel et al., 2005; Kofman et al., 2017), side view imaging (Mathie et al., 2013) or LIF intensity method (Adomeit and Renz, 2000; Alekseenko et al., 2005; Lel et al., 2005). However, a strong requirement is to measure temperature and thickness simultaneously at the same location to evidence the flow

induced by the wave motion on the heat transfer. For this reason, the same fluorescence signal is used to measure both the temperature thanks to the intensity ratio and the thickness of the liquid film thanks to the raw intensity of the fluorescence signal. The main advantages of this method are that no assumption is required to evaluate the temperature within the liquid film and that the measurement is robust enough to be used in strongly perturbed wave cases. Even if this technique does not provide as much information on the temperature distribution as an imaging technique, it can be useful to validate numerical simulations (Dietze, 2019) or low-dimensional models (Chhay et al., 2017).

After a short description of the experimental setup for heating the film and generating the waves, the technique used to measure temperature and thickness simultaneously is described. Measurements are validated against other existing techniques when available. Finally, the measurement technique is applied to a few configurations where the wave perturbation has a significant effect on the enhancement of the heat transfer.

2 Falling film experimental setup

The experimental setup, described in Figure 1, is the same that was presented by Collignon et al. (2021). The wall consists of a 100 μm thick titanium foil. The edges of the foil are clamped between two copper rods which serve as electrodes to inject an electrical current into the titanium foil and enable heating by Joule effect. The distance between the two electrodes is 30 cm, their length being 40 cm. The heat flux provided to the foil is quite uniformly distributed over the foil. Edge effects at the borders of the electrodes on the distribution of heat flux density can be neglected when measurements are performed in the middle of the foil as in the following. Copper electrodes are connected to a set of DC power, which can provide a current up to 1500 A for a 3 V voltage. The titanium foil and the two copper rods can be tilted with respect to the upstream tank to control the gravity-driven liquid flow. The liquid film is generated by the overflow of a first water tank located upstream of the heated foil. After flowing along the titanium sheet, the liquid falls into the downstream buffer tank. Thanks to a pump, the liquid is propelled through a heat exchanger in order to be cooled before being injected in the upstream tank. Since the liquid flows in a closed loop circuit, this cooling is necessary to maintain a constant temperature of the upstream fluid during the experiments. In order to limit the transmission of vibrations to the liquid, the pump and the foil setup are separately mounted on vibration dampers. A honeycomb grid is used to achieve quiescent conditions inside the upper tank. The liquid flow rate q_v is measured using an ultrasonic flow meter of precision ± 0.05 L/min. Measurement of q_v allows to determine the Reynolds number Re as follows:

$$Re = \frac{q_v}{l\nu}, \quad (1)$$

where l is the foil width ($l = 30$ cm presently) and ν is the kinematic viscosity of the liquid. Waves naturally develop at the surface of the liquid film, but a certain flow distance is necessary for these instabilities to be amplified. Given the limited length of the titanium foil, a harmonic perturbation is applied to the inlet liquid flow rate to generate the waves more rapidly. Two loudspeakers are connected to a plastic plate in contact to the liquid free surface in the upper tank. The vertical oscillation of the speakers' membrane is transmitted to the liquid and results in the onset of waves at the film surface.

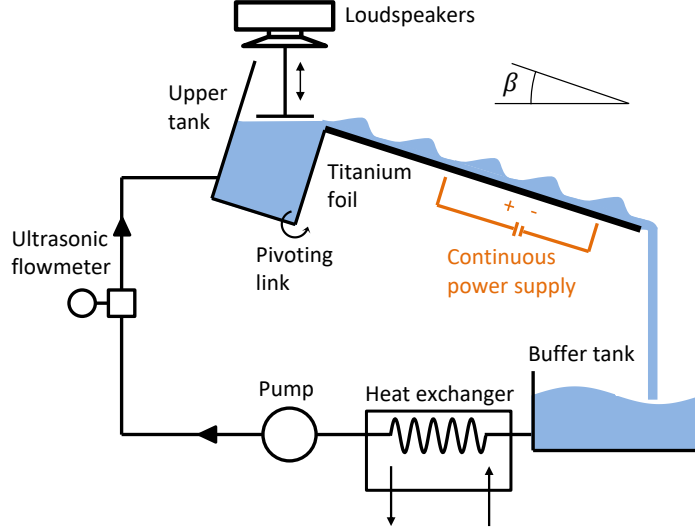


Figure 1: Scheme of the experimental set-up used to generate waves and study the heating of the falling film.

3 Temperature measurements in the falling liquid film

The temperature measurement is based on the two-colour laser-induced fluorescence technique, which has a vast range of applications in two-phase flows either as a pointwise measurement technique (Perrin et al., 2015; Stiti et al., 2019) or as an imaging technique using matrix cameras and a laser light sheet (Dunand et al., 2012; Chaze et al., 2017; Castanet et al., 2020). In the following section, the main steps of implementation of this approach to determine the temperature in thin liquid films is described.

Measurement principle

The liquid is first seeded with fluorescent molecules in very small quantity. When excited by a laser tuned on the absorption spectrum of the dye, the intensity of the fluorescence dF_λ [W] at wavelength λ produced by an elementary liquid volume dV containing the fluorescent molecules, can be expressed as:

$$dF_\lambda = K_\lambda \varepsilon_0 C \phi_\lambda I_0 dV \quad (2)$$

In this expression, K_λ is a parameter taking account light transmission throughout the liquid film and the optics as well as the solid angle for the signal collection. C [mol/m³] is the concentration of the fluorescent dye. The parameter ε_0 [m³/mol/m] denotes the absorption coefficient of the dye at the laser wavelength. ϕ_λ corresponds to the fluorescence quantum yield which is defined as the number of photons emitted by the fluorescent molecules divided by the number of photons absorbed by the same molecules. I_0 is the laser light intensity [W/m²]. Among parameters in Equation (2), only ε_0 and ϕ can be dependent on temperature (Chaze et al., 2016). The signal F received by a detector is the integration over the complete emission spectrum (Equation 2) within a measurement volume V_m .

In practice, difficulties arise from the fact that the measurement volume V_m and thus the signal F are changing with the thickness of the film. Also, light transmission (K_λ) and laser light distribution (I_0) within the film are likely to be modified by the curvature of the liquid/air surface due to effects upon light reflection and refraction. To overcome these difficulties, a ratiometric approach using two spectral bands of detection for the LIF signal is adopted. Two dyes (denoted 1 and 2 hereafter) are mixed into the water solution and their respective emissions F_1 and F_2 are detected in separate

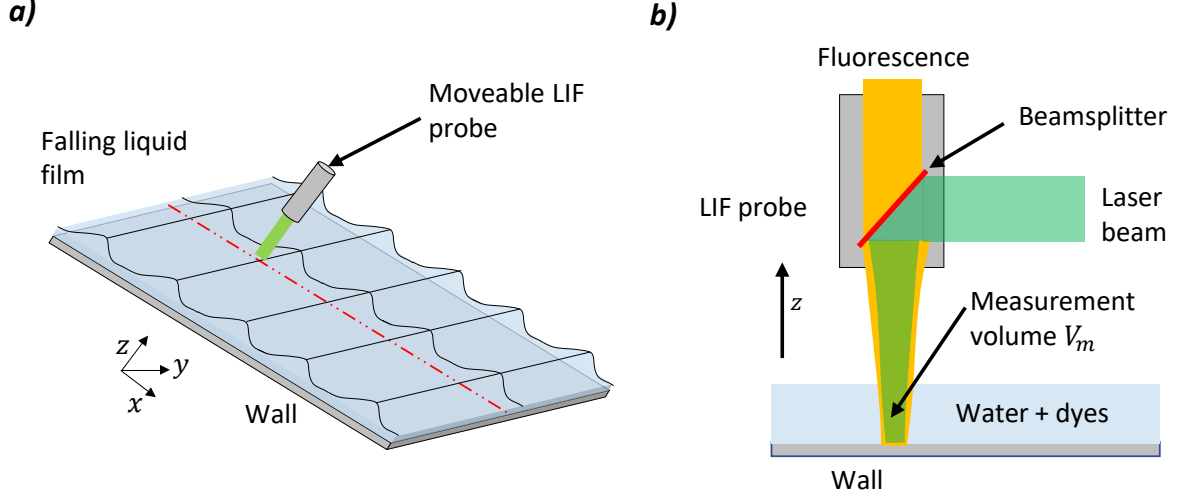


Figure 2: Schemes of the probe used to measure the LIF intensity in the liquid film. The LIF probe is displaced to perform measurements at any position (x, y) of the film (a). It transmits the excitation light from a laser and collects the fluorescence signal in the film thickness (b).

spectral bands. The intensity ratio R of these detection bands can be written as:

$$R = \frac{F_1}{F_2} = \frac{K_1 \varepsilon_{0,1} \phi_1 C_1}{K_2 \varepsilon_{0,2} \phi_2 C_2} \quad (3)$$

Advert optical effects mentioned above can be eliminated in the intensity ratio R . Although K_λ is a function of light transmission across the liquid film, the ratio K_1/K_2 is not expected to vary noticeably, since the change in refractive index of water between the two deflection bands is very small and that the absorption of light intensity through the liquid film is considered negligible. This point is further discussed later when dye concentrations choice is mentioned. Selecting two dyes with very different temperature sensitivities makes it possible to achieve a high temperature sensitivity of the ratio R . Based on a previous work by [Chaze et al. \(2016\)](#), Rhodamine 560 (Rh560) and Kiton Red (KR) were used along with a laser light excitation at 532 nm. According to [Chaze et al. \(2016\)](#), the effect of temperature on the ratio R can be described by:

$$R = R_0 \exp [(s_1 - s_2) \cdot (T - T_0)], \quad (4)$$

where $s_1 = \frac{1}{F_1} \frac{dF_1}{dT}$ and $s_2 = \frac{1}{F_2} \frac{dF_2}{dT}$ are the temperature sensitivities of dyes 1 and 2 in their respective detection bands. For Equation (4) to be valid, the emission of each dye must predominate in its respective detection band. A reference point is needed to obtain the values of R_0 and T_0 . It is usually taken under isothermal conditions, since the temperature can be easily evaluated introducing a thermocouple in the upstream or buffer tanks.

Selection of the detection bands

The measurement system developed for the purpose of this study is an optical probe which is intended to be positioned above the liquid film, normal to the wall (z direction). Laser light excitation and fluorescence collection are performed with the same optical probe as depicted in Figure 2. The probe can be moved to perform measurements at any prescribed point (x, y) of the film. As shown on Figure 3, there is a significant shift in the emission spectra of Rh560 and KR, which allows the detection of fluorescence in the following bands:

- Band 1: [496 nm - 517 nm] for the emission of Rh560,

- Band 2: [610 nm - 630 nm] for the emission of KR,

with a minimum of spectral conflicts. This means that the emission of one dye in the detection band associated to the other dye is very limited.

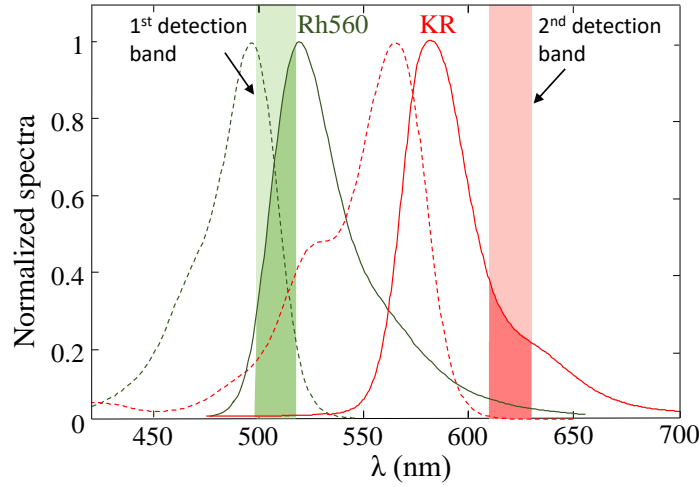


Figure 3: Emission (full lines) and absorption (dotted lines) spectra of the two fluorescent dyes used to study falling films, represented with the respective detection bands chosen for LIF measurement.

The optical measurement system

The probe configuration is comparable to an epi-fluorescence microscope. The laser light emission and the fluorescence collection are achieved with the same objective (Figure 4). However, the system is not intended for an optical slicing like in microscopy but exactly the opposite, i.e. the measurement is an integration in the entire thickness without any preferential region.

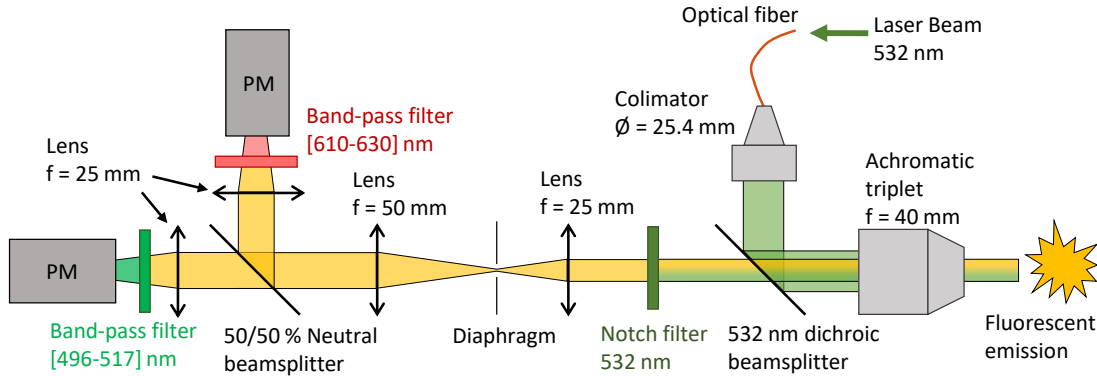


Figure 4: Optical probe used both for illumination by laser light and for collecting the fluorescence signal.

A continuous wave Nd:YAG laser beam (Quantum Laser, Finesse, $P_{max} = 12$ W, wavelength 532 nm) is transmitted by an optical fiber to the probe. Then, a lens collimator and a 532 nm dichroic beamsplitter are used to direct the laser light to an achromatic triplet. This optical arrangement is intended to allow the collimation of the laser beam and control its diameter. After the achromatic triplet, the laser beam has a very low divergence and as such it can be considered as a cylinder of diameter about 2 mm when it crosses the liquid film. This diameter roughly corresponds to the wavelength of capillary ripples, which may result in filtering the detection of ripples of low amplitudes and short wavelengths. The same achromatic triplet is used to collect the fluorescence signal. This

optical arrangement, where both the illuminated light and the emitted light pass through the same lens, minimizes the need for optical alignments especially when the probe has to be moved. However, the reflection of the laser beam on the surface of the titanium foil can be a problem. A notch filter with a high optical density avoid the laser light to go through the photo-detectors. A spatial filter composed of two convergent lenses (respectively $f = 25$ mm and $f = 50$ mm) and a diaphragm, limits the amount of parasitic light entering the optical probe. Changing the diaphragm aperture affects the light collection as well as the depth of field of the collection system. In the present work, the diaphragm aperture is reduced to have a depth of field much larger than the thickness of the film, even if this comes at the expense of the fluorescence signal. With such an approach, collection of fluorescent light is expected to have the same efficiency at all depths in the film (meaning that parameter K in Equation (2) is not changing with z). Finally, the fluorescence signal is separated in the two aforementioned spectral bands of detection, thanks to a neutral beamsplitter and two interferential bandpass filters. The fluorescence signal is detected by two photomultiplier tubes (Hamamatsu H10721-210) and the output current, amplified and converted into voltage, is transformed into digital data by an A/D acquisition board (ADLINK PCIe-9834) doing the sampling at a frequency up to 10 MHz.

Temperature measurement based on the intensity ratio

The temperature sensitivity of the two dyes was characterized in a cuvette with a control of the liquid temperature. Figure 5 shows the emission spectrum of the dyes mixture at different temperatures. The fluorescent intensity of Rh560 increases moderately with temperature, while a pronounced decrease of intensity can be observed for KR. These trends can be explained in the case of Rh560 by the fact that the absorption cross section ε_0 at 532 nm increases with temperature. For KR, the fluorescence quantum yield ϕ is decreasing with the temperature. The temperature sensitivity of each dye can be evaluated by considering an exponential function of the temperature as follows (Chaze et al., 2016):

$$F_k(T) = F_{k,0} \exp(s_k \cdot (T - T_0)), \quad \text{with } k = 1 \text{ or } 2 \quad (5)$$

From the spectra in Figure 5, the logarithm of the signal detected on each band can be plotted as a

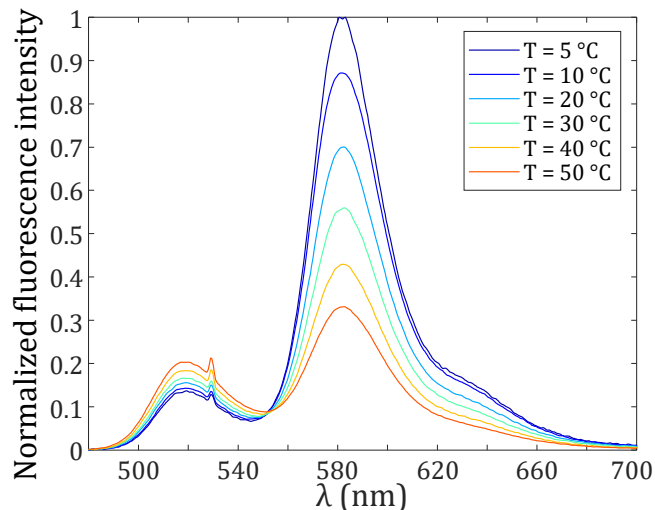


Figure 5: Evolution of the fluorescence intensity of the Rh560/KR mixture with temperature, in pure water for respective concentration $C_{Rh560} = 5 \cdot 10^{-7}$ mol/L and $C_{KR} = 5 \cdot 10^{-8}$ mol/L.

function of the temperature, which allows evaluating the temperature sensitivities s_1 and s_2 of the dyes in their respective bands of detection. In Figure 6.a, the values obtained correspond to $s_1 = +0.9\%/^{\circ}\text{C}$ and $s_2 = -2.0\%/^{\circ}\text{C}$ for Rh560 and KR respectively. These values are in good agreement with previous studies (Chaze et al., 2016). The factor $(s_1 - s_2)$ in Equation 4 can be evaluated directly from these

values of s_1 and s_2 . Nonetheless, a temperature calibration was also performed with the LIF probe for assessment (Figure 6.b).

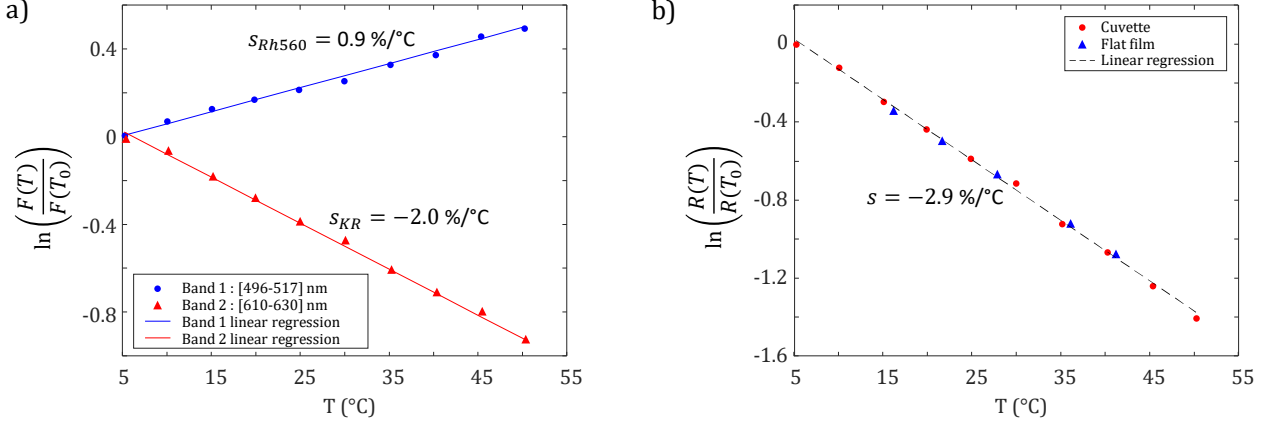


Figure 6: Temperature response of Rh560 and KR. Temperature sensitivities were evaluated for both dyes separately (a) and for the intensity ratio of the dye mixture ($C_{Rh560} = 5 \cdot 10^{-7}$ mol/L and $C_{KR} = 5 \cdot 10^{-8}$ mol/L in pure water) (b). Band 1 is attributed to Rh560 emission and band 2 is attributed to KR.

Dyes concentration

Special care was taken to limit possible effects of laser absorption and fluorescence reabsorption. These effects must be negligible to ensure that the temperature calculated from the R ratio can be assimilated to a volume average over the depth of the liquid film. Thanks to its red shift, the band [610 nm - 630 nm] is not affected by reabsorption of its signal. On the other hand, the band [496 nm - 517 nm] is absorbed by both Rh560 and KR. Absorption coefficients were measured at 20°C. Peaks of absorption are respectively $\varepsilon = 1.43 \cdot 10^7 \text{ M}^{-1} \text{ cm}^{-1}$ at 565 nm for KR and $\varepsilon = 8.96 \cdot 10^6 \text{ M}^{-1} \text{ cm}^{-1}$ at 496 nm for Rh 560. The concentration of Rh560 was fixed to $C_{Rh560} = 5 \cdot 10^{-7}$ mol/L to limit self absorption to less than 1% considering a 3 mm optical path. The concentration of KR, less critical for the problem of reabsorption, was adjusted to $C_{KR} = 5 \cdot 10^{-8}$ mol/L to have a ratio R about equal to 1 at 20°C. As for the laser light attenuation, the absorption coefficients at 532 nm are respectively $\varepsilon = 4.80 \cdot 10^6 \text{ M}^{-1} \text{ cm}^{-1}$ for KR and $\varepsilon = 1.52 \cdot 10^5 \text{ M}^{-1} \text{ cm}^{-1}$ for Rh 560, which yields an attenuation of the order of 0.1% over a distance of 3 mm.

4 Measurement of the liquid film thickness

As explained above, the optical probe can be configured in such a way that the output laser beam has little divergence and fluorescence signal is collected over a depth much larger than the film thickness. Under these conditions, the measurement volume V_m and thus the intensity of the fluorescent signal F are expected to be approximately proportional to the thickness δ of the film:

$$\delta = \delta_0 \cdot \frac{F}{F_0} \quad (6)$$

In this expression, F denotes the intensity of the fluorescence signal measured by the LIF probe in one of the two detection bands. A reference point is required to get a quantitative measurement of the film thickness δ . It consists in measuring the signal F_0 for a known thickness δ_0 of the film. In practice, a Chromatic Confocal Imaging sensor (CCI) (CHRcodile C sensor from Precitec Optronik, measurement range from 0 to 4 mm, accuracy of 1.2 μm) was used once-and-for-all to measure the thickness δ_0 of a flat unperturbed liquid film. It is placed 9.4 cm downstream of the LIF probe while

the intensity of the fluorescence signal F_0 is measured. In fact, Equation (6) is an approximation which does not consider the temperature dependence of fluorescence. For greater accuracy, a correction factor K_c is introduced in Equation (6):

$$\delta = \delta_0(T_0) \cdot \frac{F(T)}{F_0(T_0)} \cdot K_c \quad (7)$$

The reference thickness δ_0 and the reference intensity F_0 are now measured in the absence of heating when liquid temperature is uniformly equal to T_0 . K_c can be determined by:

$$K_c = \exp(-s \cdot (T - T_0)), \quad (8)$$

where s is the temperature sensitivity of the detection band considered for the thickness measurement. Alternatively, thickness can be obtained as an average measurements of bands 1 and 2:

$$\delta = \frac{\delta_0(T_0)}{2} \cdot \left(\frac{F_1(T)}{F_{1,0}(T_0)} \cdot K_{c,1} + \frac{F_2(T)}{F_{2,0}(T_0)} \cdot K_{c,2} \right) \quad (9)$$

Since KR and Rh560 have opposite temperature sensitivities, it was noticed that the approximation consisting to set the values of $K_{c,1}$ and $K_{c,2}$ to 1 in Eq. (9) can be acceptable in many cases. An example is given in Figure 7. On this figure, an estimation of the error between the temperature-corrected and uncorrected thickness measurement relative to the temperature-corrected value is also plotted. The approximation $K_{c,1} = K_{c,2} = 1$ is compared to the rigorous method where $K_{c,1}$ and $K_{c,2}$ are functions of the temperature deduced from the LIF intensity ratio R , obtained by injecting in Eq. 8 the results from the calibration shown in Fig. 6. This specific wave case was chosen out of all the explored experimental conditions, which will be discussed further, for the very steep wave front traveling along the film. As can be seen, the curves for the two evaluation methods of the film thickness are practically indistinguishable, validating in that the use of the approximation $K_{c,1} = K_{c,2} = 1$. In typical working conditions, the temperature varies only a few $^{\circ}\text{C}$ as in the example in Figure 7. As such, a negligible error is expected for all the cases which are presented hereafter.

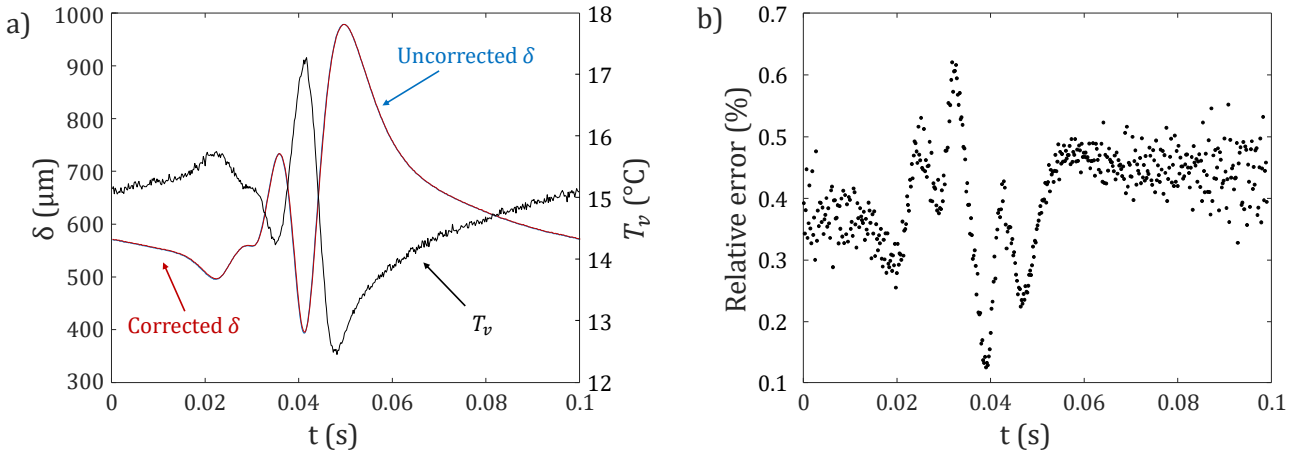


Figure 7: LIF-based film thickness measurement for $Re = 200$, $\beta = 10^{\circ}$, $f = 10$ Hz, $T_0 = 10^{\circ}\text{C}$ and $q_w = 1.25$ W/cm 2 . (a): effect of the temperature correction on the measurement of the liquid film thickness. (b): error between the temperature-corrected and uncorrected thickness measurement relative to the temperature-corrected value. The curve in black correspond to the film temperature T_v . The blue and red curves are representing the thickness of the film. The blue curve is obtained by applying Equation (9) with coefficients $K_{c,1}$ and $K_{c,2}$ equal to 1. The curve in red is the temperature-corrected thickness measurement depending on the volume average temperature using values of $K_{c,1}$ and $K_{c,2}$ prescribed in Equation (8).

5 Measurements biases and uncertainties

Before applying the previously described measurement techniques, it is critical to evaluate the possibilities of some measurement biases and quantify them. Despite the attention paid to the optical probe system and its arrangement, faults in the alignment cannot be totally ruled out. An even more critical issue relates to the effect of the waves which can affect the fluorescence signal due to several reasons:

- When light rays strike the water/air interface with a non-null angle of incidence (either laser light rays coming from the probe or fluorescence light rays emerging towards the probe), the path lengths of these rays inside the film is increased due to their refraction. The measurement volume is no longer a straight cylinder perpendicular to the wall (green zone in Figure 8). It is now depending on the inclination angle α between the free surface and the wall (Figure 8). The increase of the ray path can be evaluated at $1/\cos(\gamma)$, where γ is the angular deviation of the rays refracted at the liquid surface determined by:

$$\gamma = \alpha - \arcsin\left(\frac{n_0}{n_1}\sin(\alpha)\right), \quad (10)$$

where n_0 and n_1 are respectively the refractive index of air and water. Thanks to the phase difference between the LIF and CCI thickness measurements caused by the downstream distance between the two probes, the velocity and the wavelength of the waves can be determined. It appeared that α never exceeds 15° in our experiments, including in the region of the free surface where the slope is the steepest (i.e. the wavefront and the potential preceding capillary troughs). This moderate value of α relates to the long wavelength of the film instabilities typically ranging from 3 to 15 cm. Using Equation (10), this limit for α corresponds to $\gamma = 4^\circ$ and to an increase of the optical path length of only 0.2%, which can be neglected (Figure 8).

- Thickness measurement is based on the assumption that light is totally transmitted across the surface of the liquid film. However, if a significant amount of light is reflected, this could affect the intensity of the fluorescence signal and thus leads to an overestimation of the film thickness. This possibility can be examined using Fresnel coefficients. Light reflection has to be accounted twice, when the laser beam is entering the liquid film and when fluorescence rays leaves the film. Hence, the part of light relevant for the signal can be evaluated by introducing the global coefficient of transmission T_{tot} :

$$T_{tot} = \left(1 - R_{air/water}\right) \cdot \left(1 - R_{water/air}\right), \quad (11)$$

where $R_{air/water}$ and $R_{water/air}$ are respectively the Fresnel coefficients for the reflection in the directions air to water and water to air. These coefficients were accessed for α equals to 15° to obtain an upper limit for T_{tot} . It turns out that the variation of T_{tot} relatively to the case of a normal incidence ($\alpha=0$) does not exceed 0.012%. This is small enough to conclude that the curvature of the free surface does not significantly affect the amount of light reflected in the conducted experiments.

For validation of the technique, measurements by the LIF probe were also compared to measurements performed with CCI probe. In figure 9.a, a clear proportionality can be seen between the fluorescence signal and the film thickness measured with the CCI technique in the absence of waves, meaning that the probe settings have been properly adjusted. A good agreement was also obtained in the presence of waves as illustrated in the example presented in Figure 9.b. Unfortunately, LIF and CCI probes cannot perform measurements at the same time and the same place due to the footprints of the probes. For the test, the two probes were placed next to each other at the same downstream distance x , but about 6 cm apart in the y direction. As the waves are not purely two-dimensionnal (the wavefront being not perfectly straight in the y direction), this certainly explains the slight differences

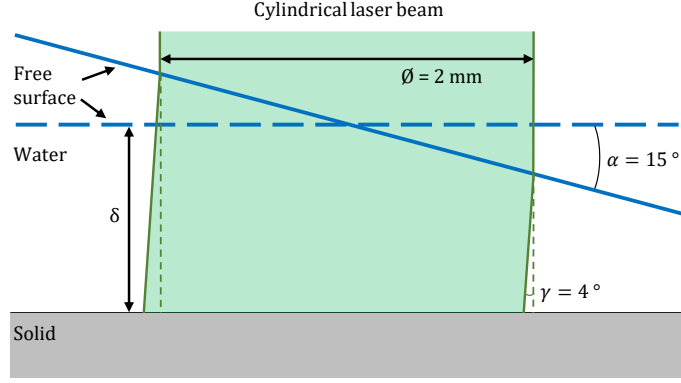


Figure 8: Deformation of the liquid volume illuminated by a laser beam of 2 mm diameter. In this illustration, the laser beam arrives vertically and passes through the air/water interface inclined at 15° to the horizontal.

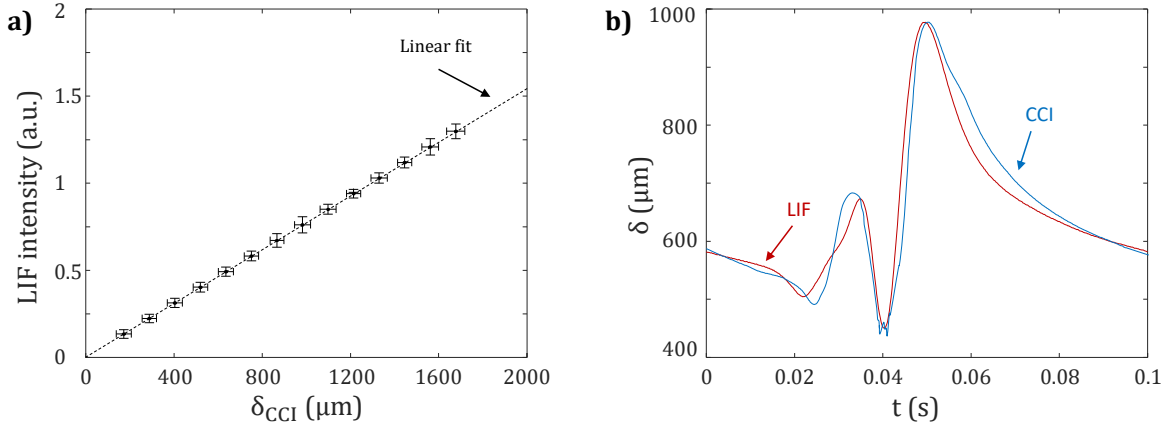


Figure 9: Evolution of the LIF signal versus the liquid thickness measured by a CCI probe for the case of a smooth liquid film (a) and comparison of the film thickness measured by LIF and CCI in the case of a wavy film in isothermal flow conditions ($Re = 200$, $\beta = 10^\circ$, $x = 180$ mm, $f = 10$ Hz and $T_v = 10^\circ\text{C}$) (b). Differences between the two techniques can be explained by the curvature of the wave front in the transverse y direction given that the waves are not purely two dimensional, due to boundary effects.

observed between the two techniques. Very similar thickness profiles are obtained overall and equally steep slopes are captured by both techniques.

Regarding temperature measurements, it is necessary to verify that the intensity ratio R totally removed the influence of the deformation of the liquid surface and the influence of the change in thickness of the film. To that end, the temperature was measured under isothermal conditions in the presence of large amplitude waves. In Figure 10, it appears that the presence of waves has a negligible effect on temperature measurements. A slight decrease of about 0.4°C - 0.6°C is systematically observed at the wave front, but this temperature deviation compares with the measurement uncertainty. From these measurements, it can be assessed that the RMS of the fluorescence ratio is close to 0.2°C , which means an uncertainty of about 0.4°C .

The previous tests allow us to conclude that the LIF probe behaves as expected. The contribution to the fluorescence signal is uniformly distributed over the entire thickness of the film, even when there are substantial surface disturbances. Therefore, the temperature measured by the LIF probe can be

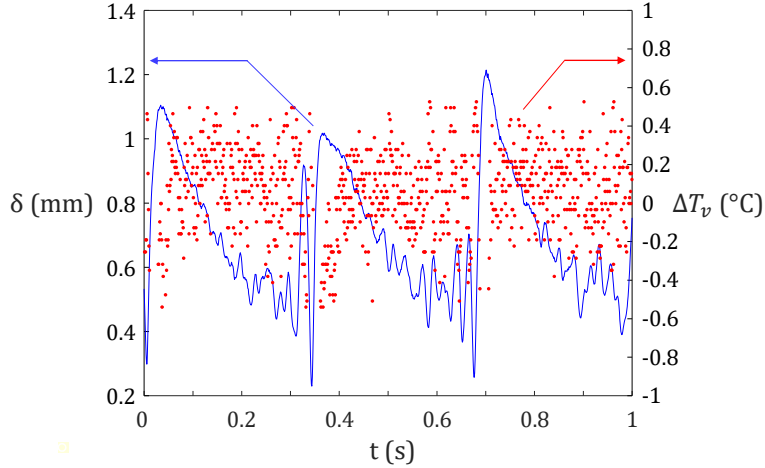


Figure 10: Temperature variation caused by the waves measured by LIF on a isothermal film ($T_v = 10^\circ\text{C}$), for $Re = 200$, $f = 3$ Hz, $\beta = 2^\circ$.

assumed to represent the volume average temperature T_v expressed as:

$$T_v(x) = \frac{1}{\delta} \int_0^{\delta} T(x, z) dz \quad (12)$$

Uncertainties in the measurements mostly arise from the noise inherent to the detection of the fluorescence signal. The signal issuing from the photomultipliers is sampled by the A/D acquisition board at 10 MHz. To improve the SNR, it was chosen to sum together packets of 10^4 points. This is equivalent to a sub-sampling at 1 kHz, but with a considerable noise reduction. This new sampling frequency remains sufficiently high compared to 10 Hz, the maximum frequency of the waves studied, so that the measurement is considered not degraded by the process. Typically after this process of averaging, the standard deviation of the signal was under 0.2% of the mean signal for each detection band. Measurements made on completely flat isothermal films suffers from a random error estimated at $\pm 0.3^\circ\text{C}$ and $\pm 5 \mu\text{m}$ on the thickness measurements. Finally, a second source of error is due to the type-K thermocouple used to measure the initial temperature of the film inside of the upper tank as a reference before heating the wall. The accuracy of this thermocouple is estimated to $\pm 0.5^\circ\text{C}$. However, reference being done one and for all, an error in the reference has no effect on the variations of temperature measured during the same experiment.

6 Results and discussion

In this section, a small number of cases are selected to illustrate the effect of the film waviness on the heat transfer coefficient (HTC). These cases correspond to exactly the same flow conditions, except for the frequency of the generated wave. A more comprehensive study is clearly desirable in the future to extend these preliminary results with an investigation of other parameters such as the Reynolds number, the inclination angle of the wall or the wall heat flux. To our best knowledge, only a few experimental studies did actually evaluate the transient evolution of HTC to evidence possible couplings with fluctuations of the film height during the wave transit, which is already a motivation for these first measurements. Moreover, none of these studies used the volume average temperature but the surface temperature to evaluate the HTC.

In the following, the liquid film is flowing over the titanium foil inclined by an angle $\beta = 10^\circ$ relative to the horizontal. The heat flux is $q_w = 1.25 \text{ W/cm}^2$ and the liquid flow rate $q_v = 3.9 \text{ L/min}$ corresponds to $Re = 200$. The initial temperature of the liquid at $x = 0$ is equal to 10°C . By changing the frequency of the loudspeaker between 2 Hz to 10 Hz, different wave height and wave profiles were

observed (Figure 11). The velocity of the waves presented here is $c_w = 0.40$ m/s. Due to the short distance available in this experiment, the waves have still not attained their saturated state. For $f = 8$ Hz, the saturation of the wave started to appear and multiple capillary waves are formed in front of the main wave front. For $f = 2$ Hz, fluctuations of the film height remains low. For $f = 10$ Hz, the wave amplitude is higher than for $f = 8$ Hz but less capillary ripples are observed. These perturbations are characterized by a prominent main wave preceded by a capillary wavelet that persists in front of the main wave for quite a long time. Time variation of the film thickness δ and averaged temperature T_v are presented for a downstream distance $x = 180$ mm. This relatively long distance (almost corresponding to the end of the foil) was chosen to allow the thermal boundary layer that develops from the heated surface to reach a sufficient height to interact with the convective wave structures. As demonstrated by Collignon et al. (2021), waves have a very limited influence on the Nusselt number when x is too small. For $f = 2$ Hz, fluctuations of the film temperature are very small which was expected given the small amplitude of the waves in that case. It is observed that the average temperature T_v is lower when the film height δ is the highest. This is consistent with previous studies pointing out that liquid is remaining cold for a longer time near the crest of the main wave (Cellier and Ruyer-Quil, 2020). For $f = 10$ Hz, still a strong correlation between the local film thickness and the temperature T_v can be evidenced. The curves for T_v and δ are roughly identical in an up-down symmetry. For $f = 8$ Hz, the same symmetry is not observed so well. The temperature decrease observed in the main wave seems smaller than expected, when comparing to the two small capillary undulations. This suggest that mixing is playing a significant role inside this wave. This could be induced by a recirculation zone in the crest region (Albert et al., 2014), but this remains to be confirmed with further investigations.

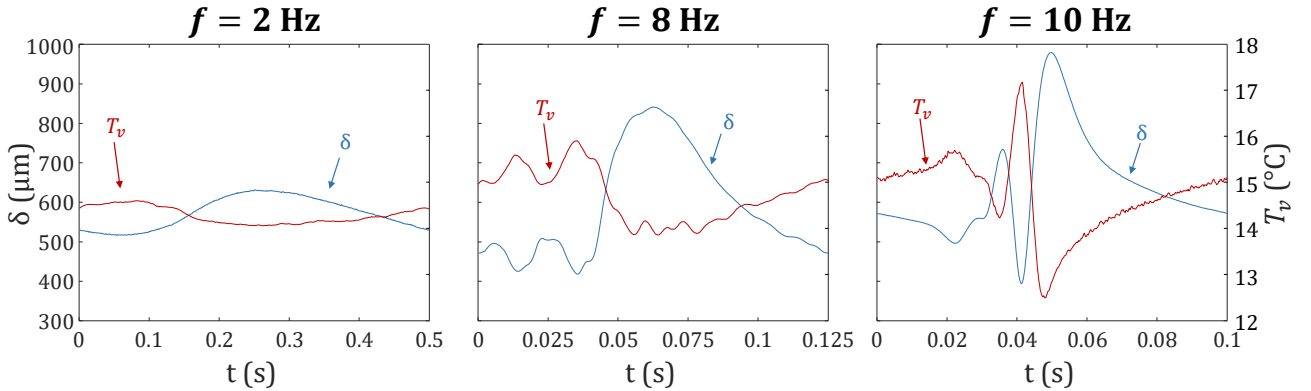


Figure 11: Time evolution of the thickness δ and of the volume average temperature T_v of the liquid film for three perturbation frequencies. Measurements were made at $x = 180$ mm, with $Re = 200$, $\beta = 10^\circ$, $x = 180$ mm, $f = 10$ Hz, $T = 10^\circ\text{C}$ and $q_w = 1.25$ W/cm².

To compare the heat transfer in these three flow configuration, the HTC is calculated as follows:

$$h_v = \frac{q_w}{T_w - T_v}. \quad (13)$$

where T_w is the temperature of the titanium foil. It is measured thanks to fifteen 0.13 mm diameter thermocouples glued along the flow to the underside of the solid wall, in the middle of the foil. Although the time response of these thermocouples is short enough to follow possible variations of the temperature, measured fluctuation of temperature proved to be negligible and a constant value of T_w can therefore be used in Equation (13). Such an observation was already made for very similar conditions in previous studies where IR thermography was used to record the wall temperature (Al-Sibai et al., 2002; Mathie et al., 2013). The effect of the film waviness can be also emphasized from a comparison to the Nusselt solution for a perfectly smooth film. Assuming a laminar and fully

developed flow, the velocity field in a perfectly smooth liquid film can be expressed as:

$$u(z) = \frac{g \sin(\beta) \delta}{2\nu} \left(\frac{2z}{\delta} - \frac{z^2}{\delta^2} \right), \quad (14)$$

where g is the acceleration of gravity and ν is the kinematic viscosity of the fluid. The temperature gradient in the flow direction can be considered to be constant for sufficiently large values of x . This means that the thermal diffusion in the x direction can be neglected, which lead to the following expression of the energy equation:

$$u \frac{\partial T}{\partial x} = a \frac{\partial^2 T}{\partial z^2}, \quad (15)$$

where a is the thermal diffusivity calculated from the liquid thermal properties $a = \lambda/\rho C_p$. Here, λ is the thermal conductivity, ρ is the density and C_p is the heat capacity of the fluid. Introducing the mean flow velocity $u_v = q_l/l$, the heat flux density at the wall q_w in a thermally developed flow can be expressed as:

$$q_w = u_v \rho C_p \delta \frac{\partial T}{\partial x} \quad (16)$$

Using Equation (14), the energy equation can be rewritten:

$$\frac{\partial^2 T}{\partial z^2} = \frac{3 q_w}{2 \lambda} \left(\frac{2z}{\delta} - \frac{z^2}{\delta^2} \right) \quad (17)$$

The boundary conditions associated to this problem are:

$$\left. \frac{\partial T}{\partial z} \right|_{z=0} = -\frac{q_w}{\lambda}, \quad T|_{z=0} = T_w. \quad (18)$$

By integrating Equation (17) twice, the liquid film temperature can be derived and the bulk temperature T_v can be evaluated by:

$$T_v = \frac{1}{\delta} \int_0^\delta T(z) dz = T_w - \frac{2 q_w \delta}{5 \lambda}. \quad (19)$$

Finally, the asymptotic Nusselt number associated to a perfectly smooth liquid film is given by:

$$Nu = \frac{h_v \delta}{\lambda} = 2.5 \quad (20)$$

The HTC predicted from this theoretical value of Nu is compared to the experimental data in Figure 12. In this figure, the HTC fluctuations caused by the waves are plotted as a function of the local film thickness. As expected, when the fluctuation of the film height is small, as for the case of $f = 2$ Hz, the Nusselt solution provides a proper estimate of the HTC. The experimental HTC is slightly decreasing with the film height and it is around the crest of the waves that the deviation from the solution $Nu=2.5$ is the largest. This deviation suggests a certain influence of the waviness on the heat transfer, although it remains very limited. For $f = 8$ Hz and $f = 10$ Hz, the relationship between h_v and δ stops being univocal as one or more loops can be observed on the plots of Figure 12. A designated value of the film thickness can correspond to several values of the HTC, meaning that the temperature gradient within the thickness of the film in the wall-normal direction is no longer purely diffusion-driven. This difference of regime is directly related to the topology of the waves. In the region marked in red in Figure 12.b, slightly higher temperatures of the film were measured when compared to other film positions with the same height, leading to a higher HTC value. This region roughly corresponds to the trough of the capillary undulations and the front region of the main wave. For $f = 10$ Hz, this observation can be related to an ascending liquid flow of higher temperature, which was experimentally evidenced by Collignon et al. (2021) in the capillary trough for a very similar case (see figure 24 in Collignon et al. (2021)). Outside the red regions mentioned above there is no singular

region in the pattern, implying a more global effect on the heat transfer. Indeed, values of h_v are distributed almost entirely above the theoretical curve of $Nu = 2.5$ for $f = 8$ Hz and $f = 10$ Hz, the most important increase is observed for $f = 8$ Hz. A careful observation of the case $f = 8$ Hz shows that the amplitude of the fluctuations of the HTC with δ is slightly smaller than for $f = 10$ Hz. Again, this means that the mixing within the liquid film attains a more efficient state. Values obtained for the HTC in Figure 12.b are difficult to compare to previous results in the literature, even if the HTC is not calculated with the volume average temperature T_v for those studies. The transient HTC inside wavy water film heated by a uniform heat flux has been experimentally determined only in a few studies. For example, [Markides et al. \(2016\)](#) and [Charogiannis and Markides \(2019\)](#) also presented their results in a diagram HTC versus δ and observed the formation of loops. For some cases they reported, a rather large amplitude of variation can be seen in their plots for HTC and δ . For some others, the variations are very little in contrast. They concluded for Re below approximately 200, that their measurement points fit very closely the prediction by the Nusselt theory of $Nu = 2.5$. In fact, the HTC depends heavily on the wave characteristics as shown previously in Figure 12, and also on the downstream distance x , if it is not long enough to suppose a thermally established flow. When the height of the waves is small, the mixing of the liquid layers is not enhanced by the waves, which seems to be the case in [Mathie et al. \(2013\)](#) for the experiments reported with a Reynolds number close to 200. This emphasizes that much work is still needed to reach a comprehensive description of the heat transfers in these wavy laminar films.

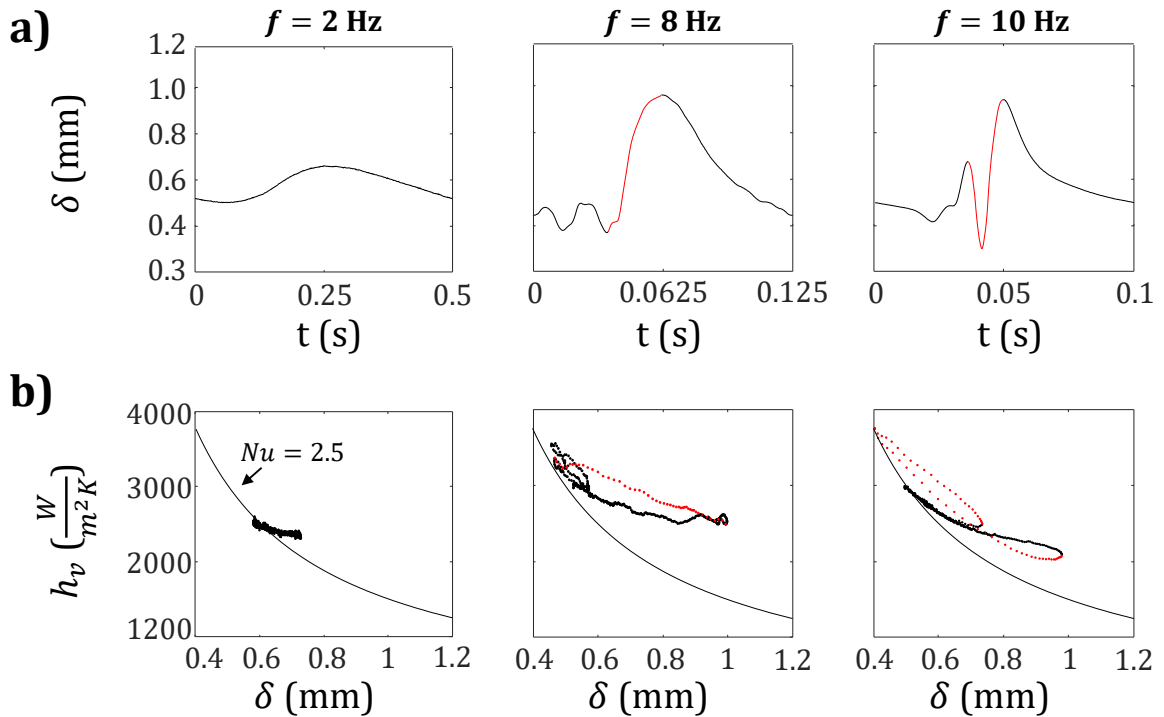


Figure 12: Evolution of the thickness δ (a) and the heat transfer coefficient h_v (b) of the falling liquid film. The heat transfer coefficient is compared to the asymptotic value of the Nusselt number of the flat film theory (black line) depending on the perturbation frequency. For the cases $f = 8$ Hz and $f = 10$ Hz, the wave front is represented on red in order to better read the curves. Measurements made at $x = 180$ mm, with $Re = 200$, $\beta = 10^\circ$, $T_0 = 10^\circ\text{C}$ and $q_w = 1.25$ W/cm^2 .

7 Conclusion

A novel measurement technique based on two-color laser-induced fluorescence was developed to obtain a simultaneous measurement of temperature and thickness of wavy liquid film flowing down an

inclined plane, without the need of any assumption concerning the temperature inside the film. The developed method is robust enough to be extended to more complex geometries, such as 3D waves cases. Regarding the temperature measurement, two fluorescent dyes with opposite temperature dependency, namely Rhodamine 560 and Kiton Red, enable a high temperature sensitivity of the fluorescence ratio used to determine the temperature after a calibration and a reference point measurement. The opposite temperature dependency of the selected dyes is exploited to limit the perturbation due to the temperature on the film thickness measurements, by simply averaging the variations of their two signals. Potential measurement biases were carefully examined. The technique proved to be weakly affected by reflection and refraction of light rays caused by the deformation of the film during the wave transit. This relates to the fact that the measurement technique is intended for thin liquid film where the wavelength of surface instabilities is much larger than the film thickness. The measurement system is a light and compact probe containing all the optical elements, designed to be easily moved atop the liquid film, whose future use in more constrained environments shall be possible. The arrangement of the optical components allows to create a probe volume of large depth normal to the inclined wall to gain access to the average temperature in the bulk of the film. The accuracy of the measurement technique is estimated to be $\pm 0.3^\circ\text{C}$ for temperature and $\pm 5\ \mu\text{m}$ for the film thickness with a time resolution of 1 ms.

The measurement technique was applied to a liquid film under several perturbation conditions to demonstrate its capability to evaluate the time evolution of the HTC. To illustrate the effect of surface waves on the enhancement of the heat transfer, the experimental data were compared with the predictions of Nusselt's theory for a smooth undisturbed film. In the case of small fluctuations of the film height, the HTC is slightly increased. For larger height fluctuations, regions of the wave where convective effects increase the heat transfer with the wall can be identified. For cases where the mixing of the liquid layers can be suspected, the HTC increases in the corresponding regions. These results provide insight into the effects related to the waviness of the film, further examination of the potential effects of many other parameters such as the Reynolds number or the distance to the flow inlet. A better understanding of the heat transfer mechanism between the heated wall and the perturbed flow deserves future studies to which this new measurement technique will be able to contribute.

Acknowledgments

The authors acknowledge support by the FRAISE project, grant ANR-16-CE06-0011 of the French National Research Agency (ANR).

References

- Adomeit, P. and Renz, U. (2000). Hydrodynamics of three-dimensional waves in laminar falling films. *International Journal of Multiphase Flow*, 26(7):1183 – 1208.
- Akesjo, A., Olausson, L., Vamling, L., and Gourdon, M. (2015). New measurement approaches for film thickness and wall temperature in falling film heat exchangers. International Conference on Heat Transfer, Fluid Mechanics and Thermodynamics.
- Al-Sibai, F., Leefken, A., and Renz, U. (2002). Local and instantaneous distribution of heat transfer rates through wavy films. *International Journal of Thermal Sciences*, 41(7):658 – 663.
- Albert, C., Tezuka, A., and Bothe, D. (2014). Global linear stability analysis of falling films with inlet and outlet. *Journal of Fluid Mechanics*, 745:444–486.
- Alekseenko, S. V., Antipin, V. A., Guzanov, V. V., Kharlamov, S. M., and Markovich, D. M. (2005). Three-dimensional solitary waves on falling liquid film at low reynolds numbers. *Physics of Fluids*, 17(12):121704–121704–4.

- Castanet, G., Caballina, O., Chaze, W., Collignon, R., and Lemoine, F. (2020). The leidenfrost transition of water droplets impinging onto a superheated surface. *International Journal of Heat and Mass Transfer*, 160:120126.
- Cellier, N. and Ruyer-Quil, C. (2020). A new family of reduced models for non-isothermal falling films. *International Journal of Heat and Mass Transfer*, 154:119700.
- Charogiannis, A. and Markides, C. N. (2019). Spatiotemporally resolved heat transfer measurements in falling liquid-films by simultaneous application of planar laser-induced fluorescence (plif), particle tracking velocimetry (ptv) and infrared (ir) thermography. *Experimental Thermal and Fluid Science*, 107:169 – 191.
- Charogiannis, A., Zadrazil, I., and Markides, C. N. (2016). Thermographic particle velocimetry (TPV) for simultaneous interfacial temperature and velocity measurements. *International Journal of Heat and Mass Transfer*, 97:589 – 595.
- Chaze, W., Caballina, O., Castanet, G., and Lemoine, F. (2016). The saturation of the fluorescence and its consequences for laser-induced fluorescence thermometry in liquid flows. *Experiments in Fluids*, 57(4):58.
- Chaze, W., Caballina, O., Castanet, G., and Lemoine, F. (2017). Spatially and temporally resolved measurements of the temperature inside droplets impinging on a hot solid surface. *Experiments in Fluids*, 58(8):96.
- Chernyavskiy, A. N. and Pavlenko, A. N. (2017). Numerical simulation of heat transfer and determination of critical heat fluxes at nonsteady heat generation in falling wavy liquid films. *International Journal of Heat and Mass Transfer*, 105:648–654.
- Chhay, M., Dutykh, D., Gisclon, M., and Ruyer-Quil, C. (2017). New asymptotic heat transfer model in thin liquid films. *Applied Mathematical Modelling*, 48:844 – 859.
- Chinnov, E. (2014). Wave – thermocapillary effects in heated liquid films at high reynolds numbers. *International Journal of Heat and Mass Transfer*, 71:106 – 116.
- Chinnov, E. and Abdurakipov, S. (2013). Thermal entry length in falling liquid films at high reynolds numbers. *International Journal of Heat and Mass Transfer*, 56(1):775 – 786.
- Chinnov, E. A. and Abdurakipov, S. S. (2017). Influence of artificial disturbances on characteristics of the heated liquid film. *International Journal of Heat and Mass Transfer*, 113:129 – 140.
- Chinnov, E. A. and Shatskii, E. N. (2010). Effect of thermocapillary perturbations on the wave motion in heated falling liquid film. *Technical Physics Letters*, 36(1):53–56.
- Chinnov, E. A., Shatskii, E. N., and Kabov, O. A. (2012). Evolution of the temperature field at the three-dimensional wave front in a heated liquid film. *High Temperature*, 50(1):98–105.
- Cohen-Sabban, J., Gaillard-Groleas, J., and Crepin, P.-J. (2001). Quasi-confocal extended field surface sensing. In *Optical Metrology Roadmap for the Semiconductor, Optical, and Data Storage Industries II*, volume 4449, pages 178–183. International Society for Optics and Photonics, SPIE.
- Collignon, R., Caballina, O., Lemoine, F., and Castanet, G. (2021). Temperature distribution in the cross section of wavy and falling thin liquid films. *Experiments in Fluids*, 62(5):115.
- Dietze, G. F. (2019). Effect of wall corrugations on scalar transfer to a wavy falling liquid film. *Journal of Fluid Mechanics*, 859:1098–1128.
- Dunand, P., Castanet, G., and Lemoine, F. (2012). A two-color planar lif technique to map the temperature of droplets impinging onto a heated wall. *Experiments in Fluids*, 52(4):843 – 856.

- Kofman, N., Mergui, S., and Ruyer-Quil, C. (2017). Characteristics of solitary waves on a falling liquid film sheared by a turbulent counter-current gas flow. *International Journal of Multiphase Flow*, 95:22 – 34.
- Lel, V., Al-Sibai, F., Leefken, A., and Renz, U. (2005). Local thickness and wave velocity measurement of wavy films with a chromatic confocal imaging method and a fluorescence intensity technique. *Experiments in Fluids*, 39:856–864.
- Lel, V., Stadler, H., Pavlenko, A., and Kneer, R. (2007). Evolution of metastable quasi-regular structures in heated wavy liquid films. *Heat and Mass Transfer*, 43(11):1121–1132.
- Lel, V. V., Kellermann, A., Dietze, G., Kneer, R., and Pavlenko, A. N. (2008). Investigations of the marangoni effect on the regular structures in heated wavy liquid films. *Experiments in Fluids*, 44(2):341–354.
- Markides, C. N., Mathie, R., and Charogiannis, A. (2016). An experimental study of spatiotemporally resolved heat transfer in thin liquid-film flows falling over an inclined heated foil. *International Journal of Heat and Mass Transfer*, 93:872 – 888.
- Mathie, R. and Markides, C. (2013). Heat transfer augmentation in unsteady conjugate thermal systems – part i: Semi-analytical 1-d framework. *International Journal of Heat and Mass Transfer*, 56(1):802 – 818.
- Mathie, R., Nakamura, H., and Markides, C. N. (2013). Heat transfer augmentation in unsteady conjugate thermal systems – part ii: Applications. *International Journal of Heat and Mass Transfer*, 56(1):819 – 833.
- Miyara, A. (1999). Numerical analysis on flow dynamics and heat transfer of falling liquid films with interfacial waves. *Heat and Mass Transfer*, 35(4):298–306.
- Perrin, L., Castanet, G., and Lemoine, F. (2015). Characterization of the evaporation of interacting droplets using combined optical techniques. *Experiments in Fluids*, 56(2):29.
- Sakakibara, J. and Adrian, R. J. (2004). Measurement of temperature field of a rayleigh-bénard convection using two-color laser-induced fluorescence. *Experiments in Fluids*, 37(3):331–340.
- Schagen, A. and Modigell, M. (2007). Local film thickness and temperature distribution measurement in wavy liquid films with a laser-induced luminescence technique. *Experiments in Fluids*, 43(2):209–221.
- Schagen, A., Modigell, M., Dietze, G., and Kneer, R. (2006). Simultaneous measurement of local film thickness and temperature distribution in wavy liquid films using a luminescence technique. *International Journal of Heat and Mass Transfer*, 49(25):5049 – 5061.
- Stiti, M., Labergue, A., Lemoine, F., Leclerc, S., and Stemmelen, D. (2019). Temperature measurement and state determination of supercooled droplets using laser-induced fluorescence. *Experiments in Fluids*, 60(4):69.
- Stiti, M., Liu, Y., Chaynes, H., Lemoine, F., Wang, X., and Castanet, G. (2021). Fluorescence lifetime measurements applied to the characterization of the droplet temperature in sprays. *Experiments in Fluids*, 62(8):174.
- Xue, T. and Zhang, S. (2018). Investigation on heat transfer characteristics of falling liquid film by planar laser-induced fluorescence. *International Journal of Heat and Mass Transfer*, 126:715 – 724.
- Yoshimura, P., Nosoko, T., and Nagata, T. (1996). Enhancement of mass transfer into a falling laminar liquid film by two-dimensional surface waves—some experimental observations and modeling. *Chemical Engineering Science*, 51(8):1231–1240.